Title: A copper(I) phosphine complex with 5,7-dinitro-2-methylquinolin-8-ol as co-ligand

Author: Jan G. Małecki, Anna Maroń, Joanna Palion, Jacek E. Nycz, Marcian Szala

Citation style: Małecki Jan G., Maroń Anna, Palion Joanna, Nycz Jacek E., Szala Marcian. (2014). A copper(I) phosphine complex with 5,7-dinitro-2-methylquinolin-8-ol as co-ligand. "Transition Metal Chemistry" (2014, iss. 7, s. 755-762), doi 10.1007/s11243-014-9857-2

UNIWERSYTET ŚLĄSKI W KATOWICACH   Biblioteka Uniwersytetu Śląskiego   Ministerstwo Nauki i Szkolnictwa Wyższego

A copper(I) phosphine complex with 5,7-dinitro-2-methylquinolin-8-ol as co-ligand

Jan G. Małecki · Anna Maroń · Joanna Palion ·
Jacek E. Nycz · Marcin Szala

Abstract 5,7-Dinitro-2-methylquinolin-8-ol has been synthesized, and its copper(I) complex has been prepared. Both the free 2-MequinNO$_2$ ligand and its complex were characterized by IR, NMR, and UV–Vis spectra. The structure of the [Cu(2-MequinNO$_2$)(PPh$_3$)$_2$] complex has been determined by single-crystal X-ray analysis. The free 2-MequinNO$_2$ ligand reveals luminescence in contrast to the complex. For 2-MequinNO$_2$, the quantum yield, lifetime of the excited state, and the rate constants of both radiative and non-radiative decay have been determined. The lack of luminescence for the complex has been explained with the use of a quantum chemical study.

Introduction

Copper(I) complexes are of interest due to their attractive photophysical properties with possible applications in solar energy conversion, electroluminescent devices, luminescence-based sensors, and biological labeling [1–3]. In Cu(I) systems, selection of the appropriate N-heterocyclic chelating ligand is the key, because it can modulate the emissive properties from the metal-to-ligand charge-transfer (MLCT) excited state [4–8]. In addition, the phosphine auxiliary ligands play a positive role in stabilizing the

J. G. Małecki (✉) · A. Maroń · J. Palion
Department of Crystallography, Institute of Chemistry,
University of Silesia, ul. Szkolna 9, 40-006 Katowice, Poland
e-mail: gmalecki@us.edu.pl

J. E. Nycz · M. Szala
Department of Organic, Organometallic Chemistry and
Catalysis, Institute of Chemistry, University of Silesia, ul.
Szkolna 9, 40-006 Katowice, Poland
e-mail: jacek.nycz@us.edu.pl

Cu(I) center, albeit they are not involved in the MLCT transitions, and also exert important effects on the photophysical properties of their Cu(I) complexes [9–11]. Emission signals from charge-transfer (CT)-excited states of copper(I) complexes are typically weak and short lived, because the lowest energy CT state of a d^{10} system involves excitation from a metal–ligand dσ* orbital [12, 13]. An important consequence is that the excited state typically prefers a tetragonally flattened geometry, whereas the ground state usually adopts a tetrahedral coordination geometry appropriate for a closed-shell ion. Aside from reducing energy content, the geometric relaxation that occurs in excited states facilitates relaxation back to the ground state. McMillin was the first to report this type of exciplex quenching, and by now, many other studies have confirmed this mechanism [14, 15]. It is well known that for typical phosphorescent [Cu(N–N)(P)$_2$] complexes, the highest occupied molecular orbital (HOMO) has predominant metal d_{Cu} character, while the lowest unoccupied orbital (LUMO) is essentially a π* orbital localized on the diimine ligand. The photoluminescence (PL) corresponds to the lowest triplet T$_1$ and is thus assigned as a ^{3}MLCT ($d_{Cu} \rightarrow \pi$*(N ligand)]. The photophysical properties of [Cu(N–N)(P)$_2$] complexes are usually sensitive toward both the structure of the ligands and the surrounding environment.

Here, we report an experimental and quantum chemical study of a copper(I) complex with a dinitro derivative of 8-hydroxyquinoline as co-ligand. This complex, as distinct from diimine copper(I) complexes, is non-emissive, although the 2-MequinNO$_2$ itself exhibits fluorescence. We have also carried out a quantum chemical study, including characterization of the electronic structure of the ground and excited states of the complex. Time-dependent density functional theory (TD-DFT) was used to calculate the electronic absorption spectrum. These results allowed for interpretation of the experimental UV–Vis spectrum and luminescence properties.

Experimental

[Cu(PPh$_3$)$_2$NO$_3$] was synthesized according to the literature method [16]. All reagents used for the syntheses of the ligand and its complex were commercially sourced and used without further purification.

Synthesis of 5,7-dinitro-2-methylquinolin-8-ol

8-Hydroxy-2-methylquinoline-7-carboxylic acid (10 g, 0.084 mol) was dissolved in concentrated H$_2$SO$_4$ (102 cm^3) at 5 °C, and a mixture of H$_2$SO$_4$ and HNO$_3$ (10 and 13 cm^3) was added dropwise at 5 °C. After stirring for 2 h, the reaction was quenched by the addition of ice (ca. 300 g), and the precipitated solid was filtered off. The crude product was crystallized from hot acetic acid to give 5,7-dinitro-2-methylquinolin-8-ol as a yellow solid.

Yield 89 %; mp. dec. = 298.7 °C; ^{1}H NMR (D$_2$SO$_4$/D$_2$O; 400.2 MHz; 70 °C) δ = 2.44 (s, 3H, CH$_3$), 7.59 (d, J = 9.1 Hz, 1H, aromatic), 8.77 (s, 1H, aromatic), 9.18 (d, J = 9.0 Hz, 1H, aromatic). IR (KBr): 1,642, 1,594 $\nu_{(C=N; C=C)}$; 1,528 $\nu_{as(NO2)}$; 1,321 $\nu_{s(NO2)}$.

UV–Vis (methanol/ethanol 1:1 v/v) [nm]: 402, 331, 290, 212, 207.

Synthesis of [Cu(2-MequinNO$_2$)(PPh$_3$)$_2$]

The copper(I) complex was synthesized in a reaction between [Cu(PPh$_3$)$_3$NO$_3$] (0.3 g, ~5×10^{-4} mol) and 5,7-dinitro-2-methylquinolin-8-ol (0.13 g, ~5×10^{-4} mol) in methanol (50 cm^3). The mixture was refluxed for 1 h. Crystals suitable for X-ray crystal analysis were obtained by slow evaporation of the reaction mixture.

[Cu(2-MequinNO$_2$)(PPh$_3$)$_2$]: Yield 63 %. Anal. Calc. for C$_{46}$H$_{36}$CuN$_3$O$_5$P$_2$: C 66.07 %; H 4.34 %; N 5.02 %; found: C 65.9 %; H 4.2 %; N 5.1 %. IR (KBr): 1,604, 1,584 $\nu_{(C=N; C=C)}$; 1,565 $\nu_{as(NO2)}$; 1,435 $\nu_{Ph(P-Ph)}$; 1,303 $\nu_{s(NO2)}$. UV–Vis (solid state) [nm]: 505, 423, 350, 260.

^{1}H NMR (500 MHz, CDCl$_3$) δ 9.56 (d, J = 8.4 Hz), 8.66 (d, J = 9.3 Hz), 8.02 (s), 6.73 (d, J = 9.3 Hz, 1H), 1.69 (s, CH$_3$).

^{13}C NMR (126 MHz, CDCl$_3$) δ 176.3 (s), 144.7 (s), 141.4 (s), 134.1 (s), 133.5 (d, J = 11.3 Hz), 132.3–131.9 (m), 129.7 (s), 128.6 (s), 124.6 (s), 113.5 (s), 22.1 (s).

^{31}P NMR (202 MHz, CDCl$_3$) δ −1.28 (s).

Physical measurements

Infrared spectra were recorded on a Nicolet iS5 FT IR spectrophotometer in the range 4,000–400 cm^{-1} using KBr pellets. Elemental analyses (C, H, and N) were obtained on a Perkin-Elmer CHN-2400 analyzer. Electronic spectra were measured on an Evolution 220 spectrophotometer in

the range of 800–200 nm, in the solid state. The ^{1}H, ^{13}C, and ^{31}P NMR spectra were obtained at room temperature in CDCl$_3$ using a Bruker 400 MHz spectrometer. Melting points were determined on MPA100 OptiMelt melting point apparatus and are uncorrected.

The steady state and time-resolved emission spectra were measured for solid samples and EtOH/MeOH (4:1) solutions on an FLS-980 spectrophotometer at ambient temperature using a Xe lamp as a light source and PMT as detector. The Raman scattering of solvents was always subtracted from the steady state emission spectra of the samples. The fluorescence was determined by absolute methods at room temperature, using an integrating sphere and solvent as a blank. The solutions of samples were first filtered and diluted to absorbance under 0.1 to avoid inner filter effect and influences of impurities from the medium, then excited at the wavelength corresponding to the excitation maximum wavelength of the compound. The time-resolved measurements were made on optically diluted (0.05 < O.D < 0.1) methanol/ethanol solutions at room temperature using time correlated single-photon counting methods. The system was aligned, and instrument response function (IRF) was designated using Ludox solution as a standard.

Cyclic voltammetry (CV) and differential pulse voltammetry (DPV) measurements were carried out on an Autolab potentiostat (Eco Chemie). A three-electrode one-compartment cell was used to contain the sample solution and supporting electrolyte in CH$_2$Cl$_2$. Deaeration of the solution was achieved by argon bubbling for about 10 min before measurement. The complex and supporting electrolyte (n-Bu$_4$NPF$_6$) concentrations were 0.0003 and 0.1 mol/dm^3, respectively. The scan rate was 0.1 V/s. A glassy carbon disk working electrode (3 mm diam.) and an Ag/Ag$^+$ reference electrode were used. The Ag/Ag$^+$ reference electrode contained an internal solution of 0.01 mol/dm^3 AgNO$_3$ in CH$_3$CN and was incorporated into the cell with a salt bridge containing 0.1 mol/dm^3 n-Bu$_4$-NPF$_6$ in CH$_2$Cl$_2$. All electrochemical experiments were carried out under ambient conditions. The UV–Vis spectroelectrochemical experiments were performed with a thin-layer cell utilizing a light transparent platinum gauze working electrode. The platinum wire counter electrode and a pseudo Ag/AgNO$_3$ reference electrode were used for the spectroelectrochemical cell. Potentials were applied and monitored with an Autolab potentiostat (Eco Chemie). Time-resolved UV–Vis spectra were recorded on an Agilent 8453 UV–Vis spectrophotometer.

Computational methods

The calculations were carried out using the Gaussian09 [17] program. The molecular geometry of the singlet ground state

Table 1 Crystal data and structure refinement details of [Cu(2-MequinNO$_2$)(PPh$_3$)$_2$]

Empirical formula	C$_{46}$H$_{36}$CuN$_3$O$_5$P$_2$
Formula weight	836.26
Temperature (K)	295(2) K
Crystal system	Monoclinic
Space group	$P2_1$/c
Unit cell dimensions	
a (Å)	9.2292(4)
b (Å)	22.5235(12)
c (Å)	19.2411(10)
α (°)	90
β (°)	90.683(5)
γ (°)	90
Volume (Å^3)	3999.4(3)
Z	4
Calculated density (Mg/m^3)	1.389
Absorption coefficient (mm^{-1})	0.677
F(000)	1,728
Crystal dimensions (mm)	0.11 × 0.11 × 0.04
θ range for data collection (°)	3.30 to 25.05
Index ranges	$-10 \leq$ h ≤ 10
	$-26 \leq$ k ≤ 26
	$-22 \leq$ l ≤ 22
Reflections collected	26,054
Independent reflections	7,052 [R_{int} = 0.0662]
Data/restraints/parameters	7,052/0/515
Goodness-of-fit on F^2	0.977
Final R indices [I > 2σ(I)]	R_1 = 0.0574
	wR_2 = 0.0762
R indices (all data)	R_1 = 0.0948
	wR_2 = 0.1335
Largest diff. peak and hole	0.365 and $-$0.307

of the complex was fully optimized in the gas phase using the B3LYP functional [18]. For the complex, a frequency calculation was carried out, verifying that the optimized molecular structure was an energy minimum; thus, only positive frequencies were expected. The 6-311+G(d,p) basis set was used to describe the copper atom, and the basis set used for the lighter atoms (C, N, O, P, H) was 6-31G with a set of "d" and "p" polarization functions. The TD-DFT method [19] was employed to calculate the electronic absorption spectrum of the complex.

Crystal structure determination and refinement

A yellow crystal of the complex was mounted on a Gemini A Ultra Oxford Diffraction automatic diffractometer equipped with a CCD detector and used for data collection. X-ray intensity data were collected with graphite monochromated MoK$_\alpha$ radiation (λ = 0.71073 Å) at 295(2) K, with ω scan mode. Ewald sphere reflections were collected up to $2\theta = 50.10°$. Details concerning crystal data and refinement are gathered in Table 1. Lorentz, polarization and empirical absorption correction using spherical harmonics implemented in the SCALE3 ABSPACK scaling algorithm [20] were applied. The structure was solved by the direct method and subsequently completed by difference Fourier recycling. All the non-hydrogen atoms were refined anisotropically using full-matrix, least-square techniques. The Olex2 [21] and SHELXS, and SHELXL [22] programs were used for all the calculations. Atomic scattering factors were used as incorporated in the programs.

Results and discussion

Spectroscopic characterization and molecular structure

The reaction of [Cu(PPh$_3$)$_2$NO$_3$] with 5,7-dinitro-2-methylquinolin-8-ol in methanol solution gave the [Cu(2-MequinNO$_2$)(PPh$_3$)$_2$] complex as a pale yellow crystalline solid. The ^{31}P NMR spectrum of the complex shows a broad singlet at -1.28 ppm, which is in agreement with the spectra of other Cu(I) PPh$_3$ complexes [23–25]. In the IR spectrum of the complex, bands with maxima at 1,565 and 1,303 cm^{-1} were attributed to asymmetric and symmetric stretching modes of the NO$_2$ groups. The C=N and C=C stretching modes of the 2-MequinNO$_2$ ligand in the complex have maxima at 1,604 and 1,584 cm^{-1}. It is worth noting a significant, hypsochromic (about 40 and 20 cm^{-1} for v_{as} and v_{as}, respectively) shift of the stretching modes of the nitro substituents in the spectrum of the copper(I) complex, compared to the free ligand. This effect suggests strong interaction between the copper center and the MequinNO$_2$ ligand.

A crystal of the complex suitable for single-crystal X-ray analysis was obtained by slow evaporation of the reaction mixture. The copper(I) ion in the complex adopts a distorted tetrahedral geometry, and the structure belongs to the monoclinic $P2_1$/c space group. The crystal structure is shown, as an *ORTEP* representation, in Fig. 1 and selected bond distances and angles are shown in Table 2. The Cu–N, Cu–O, and Cu–P bond lengths are comparable to the literature values [26, 27], as are the N(1)–Cu(1)–O(1) and P(1)–Cu–P(2) angles with values of 78.18(12) and 117.58(4), respectively. In the molecular structure of the complex, several molecular hydrogen bonds are observed and are shown in Table 3.

Quantum calculations and electronic spectra

The ground state geometries of free 5,7-dinitro-2-methyl-quinolin-8-ol and the complex were optimized in the
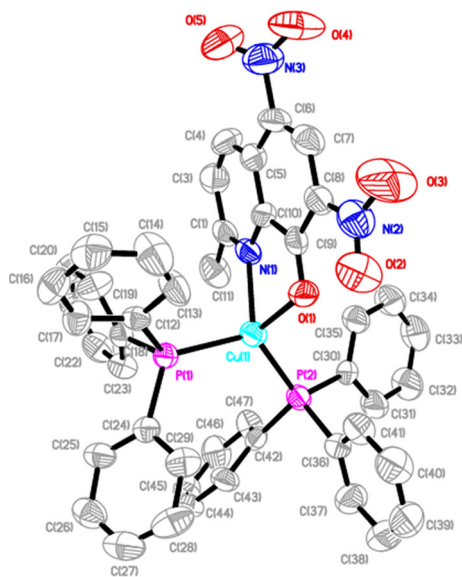
Fig. 1 *ORTEP* plot of the [Cu(2-MequinNO$_2$)(PPh$_3$)$_2$] complex. The displacement ellipsoids are drawn with 50 % probability. The hydrogen atoms are omitted for clarity

Table 2 Selected bond lengths (Å) and angles (°) for [Cu(2-MequinNO$_2$)(PPh$_3$)$_2$]

Bond lengths	Experimental	Calculated
Cu(1)–N(1)	2.103(3)	2.16
Cu(1)–O(1)	2.087(3)	2.12
Cu(1)–P(1)	2.2674(12)	2.34
Cu(1)–P(2)	2.2261(12)	2.32
Angles		
N(1)–Cu(1)–O(1)	78.18(12)	77.07
N(1)–Cu(1)–P(1)	104.75(10)	112.2
O(1)–Cu(1)–P(1)	113.29(9)	99.3
N(1)–Cu(1)–P(2)	124.57(10)	115.1
O(1)–Cu(1)–P(2)	112.27(8)	110.8
P(1)–Cu(1)–P(2)	117.58(4)	128.1

Table 3 Hydrogen bonds for [Cu(2-MequinNO$_2$)(PPh$_3$)$_2$] complex (Å and °)

D–H…A	d(D–H)	d(H…A)	d(D…A)	<(DHA)
C(4)–H(4)…O(5)	0.93	2.26	2.823(7)	118.8
C(7)–H(7)…O(4)	0.93	2.34	2.667(6)	100.2
C(13)–H(13)…O(1)	0.93	2.43	3.329(5)	161.8
C(41)–H(41)…O(1)	0.93	2.54	3.433(6)	160.1

singlet state, using the B3LYP functional. The calculation was carried out for the gas-phase molecules, and in general, the predicted bond lengths are over-estimated by about 0.1 Å. From the data shown in Table 2, one may see that

the major differences between the experimental and calculated geometries are found in the O(1)–Cu(1)–P(1) and P(1)–Cu(1)–P(2) angles, probably due to negligence of effects such as the hydrogen bonding interactions observed in the solid state. In order to verify the assignment of the electronic spectrum of the complex, the frontier orbitals were calculated at the B3LYP/6-311G(d,p) level on the basis of the crystal structural data by using the Gaussian 09 package.

As shown in Fig. 2, the results of density functional theory (DFT) calculations for the complex reveal that the electronic density in the HOMO is distributed over the 2-MequinNO$_2$ ligand, copper, and phosphorus atoms with percentage contributions for the electronic density, calculated with use of the GaussSum program [28], equal to 63, 17, and 20 %, respectively. The LUMO has the π* orbital character of 2-MequinNO$_2$, and it is distributed over the quinoline ring (64 %) with a significant share, equal to 34 %, on the –NO$_2$ group in position 5. Therefore, it is reasonable that the low-energy absorption band of the [Cu(2-MequinNO$_2$)(PPh$_3$)$_2$] complex can be assigned to mixed ligand-to-ligand charge transfer/interligand charge transfer (LLCT/ILCT) with a contribution from metal-to-ligand charge-transfer (MLCT) transitions. In particular, this is visible in solution where the maximum of this band is bathochromically shifted by only 20 nm compared with free 2-MequinNO$_2$ as shown on Fig. 3. TD-DFT calculations based on singlet orbitals showed that the electronic character of the absorption is dominated by one-electron transition from HOMO to LUMO (weight of the leading configurations, 92 %), and the calculated HOMO–LUMO gap of 2.58 eV (480 nm) is consistent with the experimental results described as LLCT/ILCT mixed with MLCT transition character. The calculation of the electronic structure of 5,7-dinitro-2-methylquinolin-8-ol shows that the LUMO is mainly localized on the NO$_2$ group at position 7 with the percentage of contribution equal to 68 %, while the lower occupied and upper unoccupied (HOMO−1, HOMO−2, LUMO+1, LUMO+2) are composed of quinoline ring orbitals. The calculated energy of the HOMO–LUMO transition equal to 411 nm agrees with the experimental data. Figure 4 presents the frontier orbitals of the free ligand and the complex. The complex both in the solid state and solution does not give emission, as distinct from the 5,7-dinitro-2-methylquinolin-8-ol which when excited (in solution) at 332 nm reveals luminescence with a maximum at 372 nm and quantum yield of 0.0043. The lifetime of the excited state is about 5.5 ns, and the rate constant of radiative decay, calculated on the basis of the lifetime and quantum yields, i.e.,

$$\tau = \frac{1}{k_r + k_{nr}} \quad \text{and} \quad \Phi = \frac{k_r}{k_r + k_{nr}}$$
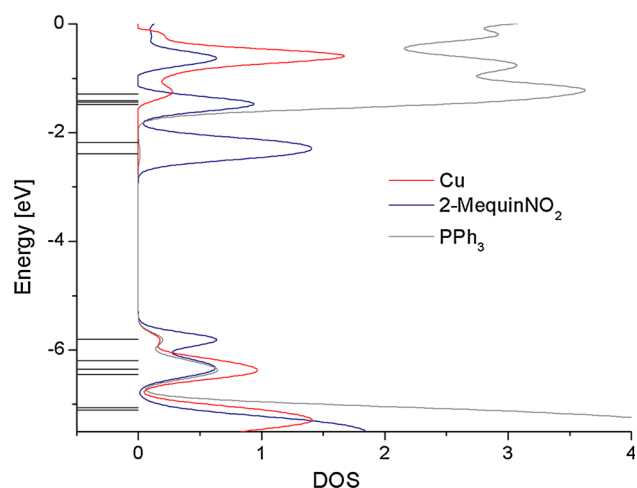
Fig. 2 Density-of-states diagram for [Cu(2-MequinNO$_2$)(PPh$_3$)$_2$] complex
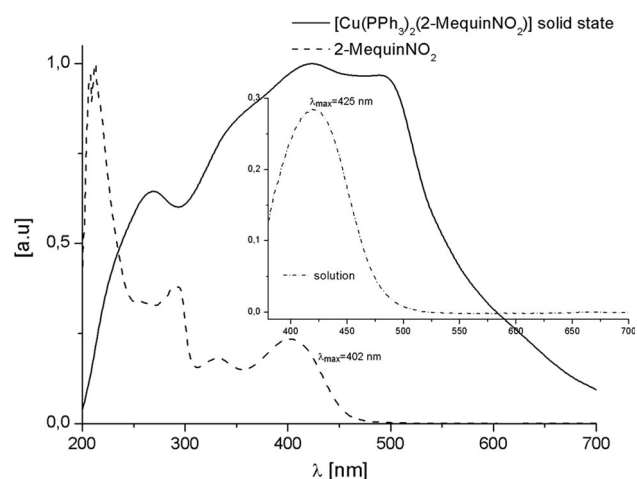
Fig. 3 UV–Vis spectra of solid state (*solid line*), methanol–ethanol solution of [Cu(2-MequinNO$_2$)(PPh$_3$)$_2$] complex (*inset*) and solution of 2-MequinNO$_2$ ligand (*dash line*)

is considerably smaller (7.788×10^5 s^{-1}) than the non-radiative decay (1.803×10^8 s^{-1}) process. The excitation wavelength corresponds to transitions in which molecular orbitals localized on the quinoline ring play a significant role. In this energy range, HOMO → LUMO (55 %) and HOMO−2 → LUMO+1 (40 %) transitions were calculated. The prevalence of the HOMO → LUMO transition in excitation may be the reason for predominance of non-radiative decay of the excited state for the sake of substantial participation of –NO$_2$ substituents in the LUMO (Fig. 5).

The lack of luminescence in the case of the complex may be connected with its electronic density distribution. In this case, NO$_2$ group in position 5 is engaged in the LUMO and also contributes to the higher virtual orbitals

(LUMO+1 to LUMO+3 with percentage of 11 %) as distinct from free 5,7-dinitro-2-methylquinolin-8-ol in which –NO$_2$ in the *ortho* position plays a role. Therefore, the nitro substituent in position 5 (*para*) perturbs greatly the electronic structure (more electron withdrawing in the position 5 than in the position 7) of the complex, resulting in the non-radiative decay of excited states.

Electrochemistry

The electrochemical characterization of the complex has been performed by cyclic voltammetry and differential pulse voltammetry (DPV) in dichloromethane/n-Bu$_4$NPF$_6$ solutions in the potential range of −2.2 to 1.5 V at a scan rate 0.1 V/s with Ag/Ag$^+$ reference electrode. The ferrocene/ferrocenium (Fe/Fe$^+$) electrode was used as an internal standard. The ferrocene/ferrocenium reversible couple reported versus Ag/Ag$^+$ was observed at 0.074 V with peak potential separation 64 mV. The CV and DPV spectra are shown in Fig. 6, and in Table 4, the electrochemical properties of the complex are shown. As one can see, the complex displays one quasi-reversible pair for each oxidation and reduction process. Their quasi-reversibility is proved by the peak-to-peak separation ($\Delta E > 100$ mV). Additionally, irreversible oxidation and two irreversible reductions are visible. The Cu(II)/Cu(I) couple appears at 0.82 V. The irreversible response observed at 1.46 V is probably connected with oxidation within the phosphine ligands. For a Cu(I) complex, phosphine oxidation occurs at more positive potentials than for free PPh$_3$ because of electrostatic and inductive effects (free PPh$_3$ in acetonitrile showed a single anodic peak at 1.00 V). The response at negative potential at −1.72 V is assigned to reduction of the 2-MequinNO$_2$ ligand which is consistent with the relatively low-lying nature of the quinoline π^* orbitals. The reduction process occurs at potential values very similar to those reported earlier for Cu(I) complexes with phenanthroline ligands [29].
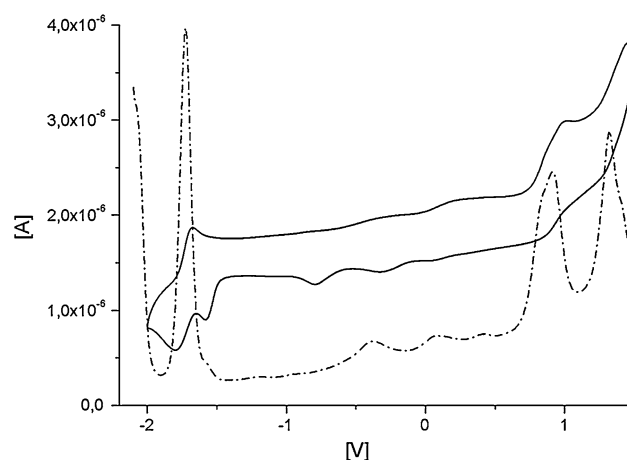
The spectroelectrochemical behavior of the complex was investigated using an in situ technique including chronoamperometry and UV–Vis spectroscopy in an acetonitrile solution containing 0.1 M n-Bu$_4$NPF$_6$. The convenient applied potential value for this experiment was obtained as $E_{app} = 1.1$ V from the CV in a thin-layer cell. The UV–Vis spectral changes for the oxidized species of the complex obtained in a thin-layer cell with the applied potential are presented in Fig. 7. During the oxidation process, the band at 423 nm decreases and the maximum is shifted to 390 nm; moreover, a new band appears at 330 nm and the band at 260 nm disappears. The observed spectroscopic changes are reversible upon re-reduction, demonstrating that on the time scale of the spectroelectrochemical experiment a chemical reaction is coupled to

Fig. 4 HOMO and LUMO contours of 2-MequinNO$_2$ and [Cu(2-MequinNO$_2$)(PPh$_3$)$_2$] complex

2-MequinNO$_2$

[Cu(2-MequinNO$_2$)(PPh$_3$)$_2$]

HOMO

LUMO
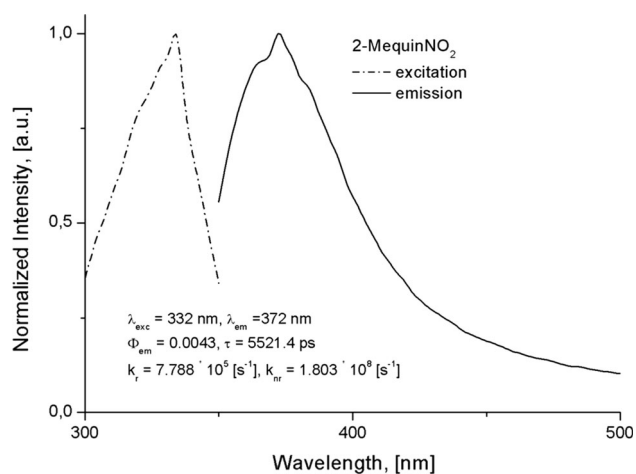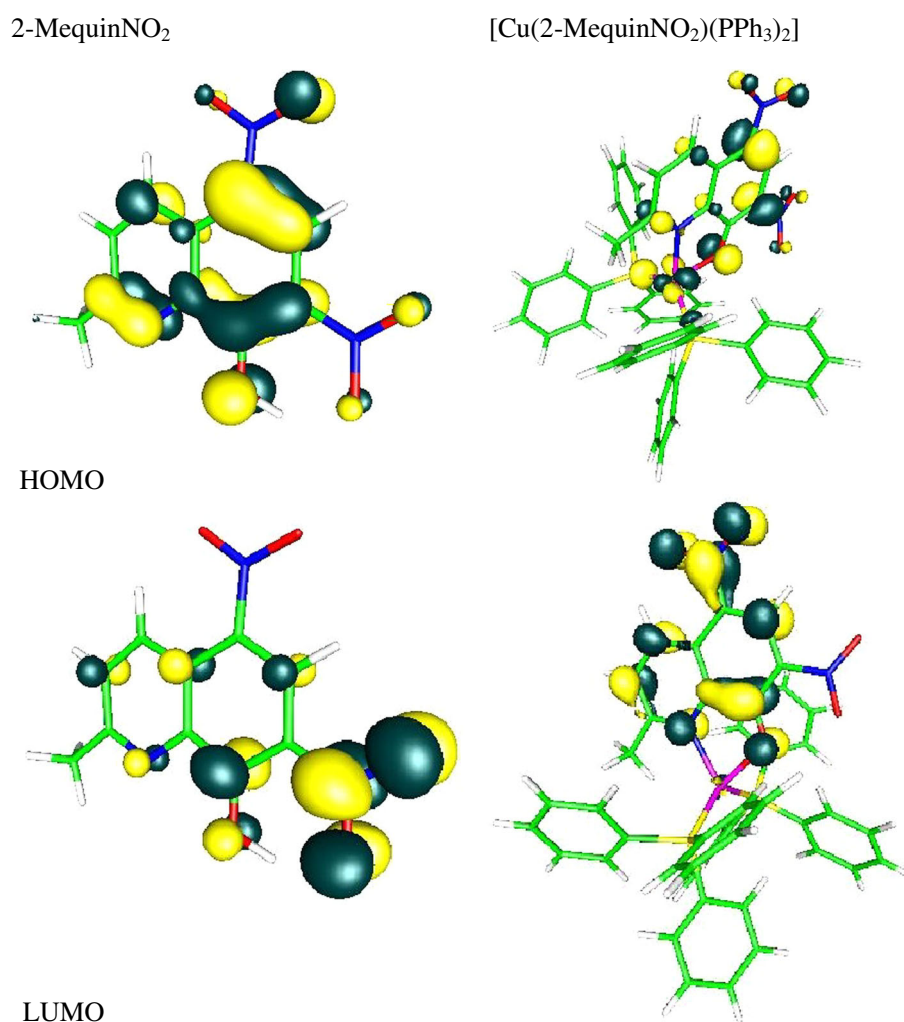
Fig. 5 Excitation and emission spectra of 5,7-dinitro-2-methylquinolin-8-ol methanol–ethanol (1:1 v/v) solution

Fig. 6 CV (*solid line*) and DPV (*dash-dot line*) spectra of the [Cu(2-MequinNO$_2$)(PPh$_3$)$_2$] complex

ligand oxidation. No other absorption band in the Vis–NIR region has been observed, ruling out the possibility of observing electronic transitions due to metal center
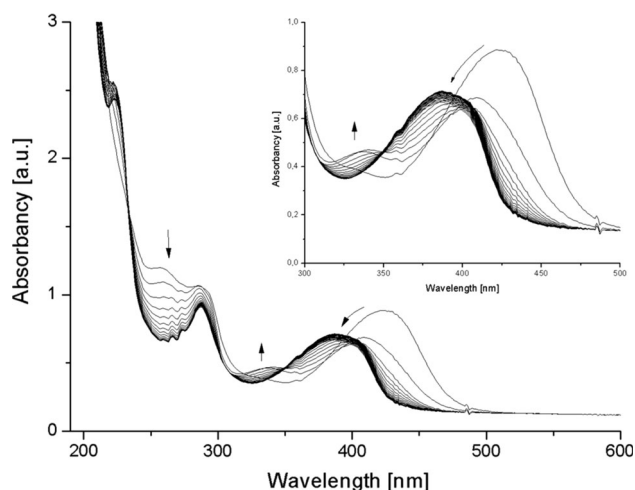
interactions. Additionally, it is known that the tetragonal copper(I) complexes upon electrochemical or photoexcitation oxidation processes undergo a flattening distortion.

Table 4 Electrochemical properties of the [Cu(2-MequinNO₂)(PPh₃)₂] complex

Method	E_{ox} (V), (ΔE [mV])	E_{red} (V), (ΔE [mV])	E_{HOMO} (eV)		E_{LUMO} (eV)		Eg^{CV} (eV)	Eg^{DFT} (eV)
			CV	DFT	CV	DFT		
CV	0.82 (319)	−1.72 (110)	−5.62	−5.89	−3.08	−2.89	−2.54	2.99
	1.46	−1.58						
		−0.79						
DPV	0.91	−1.72	−5.71		−3.08		2.63	
	1.32	−1.18						

Fig. 7 Absorption spectra of [Cu(2-MequinNO₂)(PPh₃)₂] complex in an acetonitrile/TBAP solution recorded during a spectroelectrochemical experiment corresponding to monooxidation of the complex

In the flattened geometry, the highest filled d$_{xz}$ and d$_{yz}$ orbitals of the metal have dσ* character with respect to the 8-quinolinol lone pairs. Therefore, wider P–Cu–P angles may ease dσ* interactions and in so doing enhance the energy required for CT excitation. Hence, upon oxidation the lowest energy band is hypsochromically shifted. On the other hand, the 2-MeqiunNO₂ ligand due to the strongly electron withdrawing –NO₂ substituents prevents the oxidation of the copper(I) ion.

Conclusion

5,7-Dinitro-2-methylquinolin-8-ol and its complex [Cu(2-MequinNO₂)(PPh₃)₂] were synthesized and characterized by IR, NMR, UV–Vis, and emission spectroscopy, and the complex also by X-ray crystallography. The electronic structures of the free ligand and its complex have been determined using DFT. On the basis of our analysis, it has been demonstrated that the differences in the electronic structures of the free ligand and the complex have major influences on their spectroscopic properties and determine

their fluorescence properties. The cyclic voltammetry and differential pulse voltammetry studies are in agreement with the calculated electronic structure of the complex.

Supplementary data

CCDC 972979 contains the supplementary crystallographic data for [Cu(2-MequinNO₂)(PPh₃)₂] complex. This data can be obtained free of charge from http://www.ccdc.cam.ac.uk/conts/retrieving.html, or from the Cambridge Crystallographic Data Centre, 12 Union Road, Cambridge CB2 1EZ, UK; fax: (+44) 1223-336-033; or e-mail: deposit@ccdc.cam.ac.uk.

References

1. Armaroli N, Accorsi G, Cardinali F, Listorti A (2007) Top Curr Chem 280:69
2. Ford PC, Cariati E, Bourassa J (1999) Chem Rev 99:3625
3. Bessho T, Constable EC, Graetzel M, Redondo AH, Housecroft CE, Kylberg W, Nazeeruddin MK, Neuburger M, Schaffner S (2008) Chem Commun 32:3717
4. Perruchas S, Goff XFL, Maron S, Maurin I, Guillen F, Garcia A, Gacoin T, Boilot J-P (2010) J Am Chem Soc 132:10967
5. Armaroli N, Accorsi G, Holler M, Moudam O, Nierengarten J-F, Zhou Z, Wegh RT, Welter R (2006) Adv Mater 18:1313
6. Zhang Q, Zhou Q, Cheng Y, Wang L, Ma D, Jing X, Wang F (2004) Adv Mater 16:432
7. Nishikawa M, Nomoto K, Kume S, Inoue K, Sakai M, Fujii M, Nishihara H (2010) J Am Chem Soc 132:9579
8. Chen J-L, Wu B, Gu W, Cao X-F, Wen H-R, Hong R, Liao J, Su B-T (2011) Transit Met Chem 36:379
9. Cuttell DG, Kuang SM, Fanwick PE, McMillin DR, Walton RA (2002) J Am Chem Soc 124:6
10. McCormick T, Jia W-L, Wang S (2006) Inorg Chem 45:147
11. Smith CS, Branham CW, Marquardt BJ, Mann KR (2010) J Am Chem Soc 132:14079
12. McMillin DR, McNett KM (1998) Chem Rev 98:1201

13. Armaroli N (2001) Chem Soc Rev 30:113
14. Eggleston K, McMillin DR, Koenig KS, Pallenberg AJ (1997) Inorg Chem 36:172
15. Cunningham T, Cunningham KLH, Michalec JF, McMillin DR (1999) Inorg Chem 38:4388
16. Gysling HJ (1979) Inorg Synth 19:92
17. Gaussian 09, Revision A.1, Frisch MJ, Trucks GW, Schlegel HB, Scuseria GE, Robb MA, Cheeseman JR, Scalmani G, Barone V, Mennucci B, Petersson GA, Nakatsuji H, Caricato M, Li X, Hratchian HP, Izmaylov AF, Bloino J, Zheng G, Sonnenberg JL, Hada M, Ehara M, Toyota K, Fukuda R, Hasegawa J, Ishida M, Nakajima T, Honda Y, Kitao O, Nakai H, Vreven T, Montgomery JA, Jr., Peralta JE, Ogliaro F, Bearpark M, Heyd JJ, Brothers E, Kudin KN, Staroverov VN, Kobayashi R, Normand J, Raghavachari K, Rendell A, Burant JC, Iyengar SS, Tomasi J, Cossi M, Rega N, Millam JM, Klene M, Knox JE, Cross JB, Bakken V, Adamo C, Jaramillo J, Gomperts R, Stratmann RE, Yazyev O, Austin AJ, Cammi R, Pomelli C, Ochterski JW, Martin RL, Morokuma K, Zakrzewski VG, Voth GA, Salvador P, Dannenberg JJ, Dapprich S, Daniels AD, Farkas O, Foresman JB, Ortiz JV, Cioslowski J, Fox DJ (2009) Gaussian, Inc., Wallingford, CT
18. Becke D (1993) J Chem Phys 98:5648
19. Casida ME (1996) In: Seminario JM (ed) Recent developments and applications of modern density functional theory, theoretical and computational chemistry, vol 4. Elsevier, Amsterdam, p 391
20. CrysAlis RED, Oxford Diffraction Ltd., Version 1.171.29.2
21. Dolomanov OV, Bourhis LJ, Gildea RJ, Howard JAK, Puschmann H (2009) J Appl Cryst 42:339
22. Sheldrick GM (2008) Acta Cryst A64:112
23. McCormick T, Jia W-L, Wang S (2006) Inorg Chem 45:147–155
24. Jia WL, McCormick T, Tao Y, Lu J-P, Wang S (2005) Inorg Chem 44:5706–5712
25. Min J, Zhang Q, Sun W, Cheng Y, Wang L (2011) Dalton Trans 40:686–693
26. Floriani C, Fiaschi P, Chiesi-Villa A, Guastini C, Zanazzi PF (1998) J Chem Soc Dalton Trans 1607–1615
27. Chen Z-F, Li B-Q, Xie Y-R, Xiong R-G, You X-Z, Feng X-L (2001) Inorg Chem Commun 4:346
28. O'Boyle NM, Tenderholt AL, Langner KM (2008) J Comp Chem 29:839
29. Armaroli N, Accorsi G, Bergamini G, Ceroni P, Holler M, Moudam O, Duhayon C, Delavaux-Nicot B, Nierengarten J-F (2007) Inorg Chim Acta 360:1032–1042